Synchrotron Diffraction Study of Deformation Mechanisms in Mineralized Tendon

H. S. Gupta,[1] P. Messmer,[2] P. Roschger,[2] S. Bernstorff,[3] K. Klaushofer,[2] and P. Fratzl[1]

[1]*Max Planck Institute of Colloids and Interfaces, Department of Biomaterials, 14424 Potsdam, Germany*

[2]*Ludwig Boltzmann Institute of Osteology, 4th Medical Department, Hanusch Hospital & UKH Meidling, Vienna, Austria*

[3]*Sincrotrone Trieste S.C.p.A, 34012 Basovizza, Trieste, Italy*

(Received 16 January 2003; published 4 October 2004)

The high stiffness and toughness of biomineralized tissues are related to the material deformation mechanisms at different levels of organization, from trabeculae and osteons at the micrometer level to the mineralized collagen fibrils at the nanometer length scale. Quantitatively little is known about the sub-micrometer deformation mechanisms under applied load. Using a parallel-fibred mineralized tissue from the turkey leg tendon as a model for the mineralized collagen fibrils, we used *in situ* tensile testing with synchrotron x-ray diffraction to measure the average fibril deformation with applied external strain. Diffraction peak splitting occurred at large strains, implying an inhomogeneous elongation of collagen fibrils. Scanning electron microscopy measurements lead us to conclude that the inhomogeneous mineralization in mineralized tendon is at the origin of the high fracture strain.

DOI: 10.1103/PhysRevLett.93.158101 PACS numbers: 87.64.Bx, 62.20.Mk, 68.37.Hk, 87.15.La

The molecular and microstructural basis for deformation and fracture in bone is a question of general interest not only to medicine but also in the physical sciences [1,2]. Bone is hierarchically structured, with building blocks from the molecular to the organ level [3,4], whose deformation under external stress can involve several different length scales [5]. *In situ* probes of structural changes down to the micron length scale have provided insight into deformation mechanisms such as cement line creep [6], lamellar microcracking [7,8], and intralamellar damage [9] in the osteons and lamellae. However, much less is known quantitatively about the *in situ* changes at the submicron level, where the bone matrix consists of arrays and bundles of collagen fibrils, embedded with mineral nanocrystals (carbonated apatite). This is partly because of the structural complexity at this level, with the fibrils in bone lamellae consisting of several sublayers forming a complex rotated plywood type structure [10,11].

The mineralized turkey leg tendon (hereafter MTLT) is a widely studied model tissue for mineralized collagen [12,13], where the submicron level has a much simpler parallel-fibered structure than in bone. The fibrils aggregate parallel to each other to form fiber bundles, which in turn lie approximately parallel to the tendon axis. The essentially one-dimensional geometry of the tendon makes the interpretation of the mechanical and diffraction data easier and avoids the complexity arising from the higher order hierarchical levels found in bone. While not initially mineralized, it undergoes progressive calcification from 10–12 weeks of age, along the distal to proximal direction, probably as a result of energy storage requirements and a physiological stress-induced calcification [14–16].

By using *in situ* mechanical testing with time-resolved small angle x-ray diffraction we investigated the structural changes in the mineralized collagen fibrils in MTLT tissue during application of uniaxial external stress. The technique enables the simultaneous measurements of structural changes at the macroscopic, fibrillar, and molecular levels during mechanical loading by measuring changes in diffraction patterns with time arising from straining of ordered structures at these different length scales [17–22]. Since adjacent collagen molecules in a fibril are laterally shifted by $D = 64 - 67$ nm along the fibril axis, resulting in regions of alternating high and low molecular density [23], a series of Bragg peaks with spacing $2\pi/D$ in the small angle x-ray diffraction regime can be observed in reciprocal space [24]. The changes in axial periodicity D with applied loads provide a measure of the fibril strain.

Tensile measurements were carried out in a specially designed apparatus as shown in Fig. 1. A load cell (ALD-Mini-UTC, A. L. Design Inc.) with nominal load 12.5 kg was mounted on one grip while the other was moved with a motorized translation stage (M-125.10, Physik Instrumente GmbH). To maintain the tendon in a native state the sample was partially immersed in a physiological solution of phosphate buffered saline (PBS) during the test. To prepare the samples, 0.1–0.4 $mm^2 \times 5$–10 mm long tendon strips were sectioned (under running water) along the tendon long axis, from the mineralized parts of digital flexor tendons from 12, 15, and 24 week old domestic turkeys, using a diamond saw microtome (Leica SP1600, Leica Microsystems GmbH). Sample dimensions were measured with the micrometer drive on the microtome and under a light microscope. The tendons were fixed to sandblasted metal clamps with Bond-It!^{TM} primer and Flow-It Flowable^{TM} amalgam (Jeneric-Pentron GmbH). MTLT samples were then stretched to failure at constant strain rates ranging from 0.01 to 0.1% sec^{-1} during synchrotron small angle x-ray diffraction measurements at BL 5.2 (SAXS), Sincrotrone Trieste, in Trieste, Italy (12 weeks ($n = 5$),

 © 2004 The American Physical Society

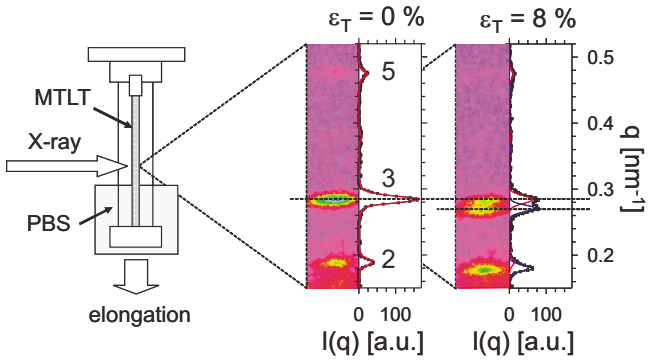

FIG. 1 (color online). *In situ* tensile testing of MTLT in phosphate buffered solution (PBS) combined with synchrotron x-ray diffraction. Right : Meridional diffraction patterns (2D spectra and integrated 1D) for macroscopic strains ε_T of 0% and 8% (Fibril axis vertical, 2nd, 3rd, and 5th orders shown).

15 weeks ($n = 6$), 24 weeks ($n = 4$)). A 2D CCD detector (Bruker AXS GmbH) at a sample-detector distance of 257.5 cm and beam wavelength $\lambda = 0.154$ nm was used to measure the diffraction frames, which were fitted with PeakFit version 4 (SPSS Inc). Synchrotron damage effects were controlled by monitoring changes in load and diffraction data after prolonged ($\geq$20 min) exposure to the x-ray beam under load, followed by attenuating the beam intensity with layers of aluminum foil for the main set of measurements.

As shown in Fig. 1, the most striking result was a peak splitting of the diffraction spectrum for large macroscopic tendon strains ε_T ($\geq$2–3%). The splitting implies an inhomogeneous fibril elongation, with part of the fibrils relaxed back to their unstressed length and the remainder elongated by more than 4–5%. The onset of peak splitting occurs shortly after the mechanical transition from approximately linear elastic to inelastic behavior in the stress-strain curve (Fig. 2). The mechanical transition point shown is defined to be the intersection of the line drawn tangent to the initial slope and the line drawn tangent to the final slope, before drops in stress at constant strain occur, implying macroscopic fracture. For tendon strains below the transition point the diffraction pattern cannot be decomposed into the sum of two different Bragg patterns, and the fibril elongation D is thus considered homogeneous in the linear elastic regime. For strains above the transition the relaxed and extended groups of fibrils have fibril staggers D_1 and D_2 ($D_1 \leq D_2$), respectively. While D_1 relaxes back to near the zero stress value of the fibril stagger D_0 ($D_0 \cong 66.4$ nm, the lateral stagger of collagen molecules), D_2 stretches to values of up to 70 nm. The value of $D_0 \approx 66.4$ nm was intermediate between the D-period value for unmineralized collagen ($D_0 = 67$ nm) and that of mineralized collagen ($D_0 = 64$ nm), probably due to the intermediate stage of mineralization of the whole tissue. In the oldest 24 week samples the peaks were closer together at maximum strain, showing a lesser degree of inhomogenous deformation.

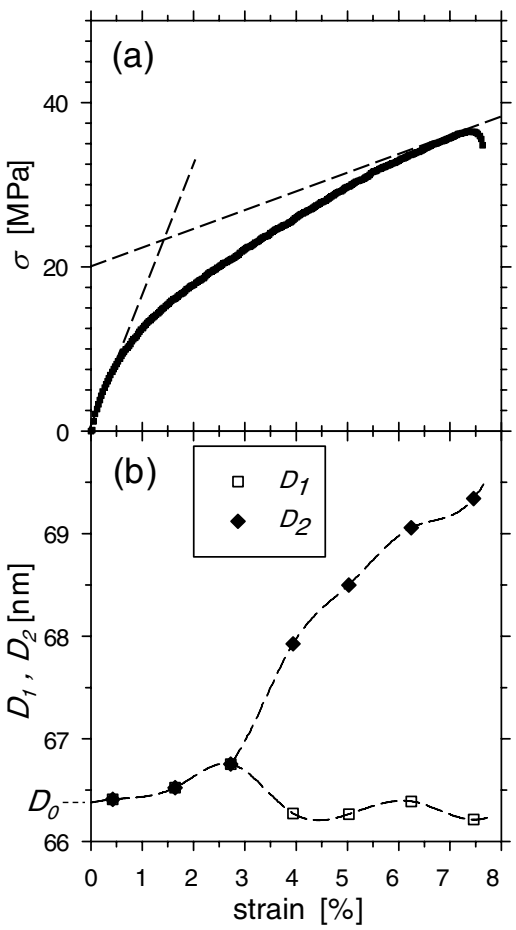

FIG. 2. Change in (a) the applied stress σ and (b) fibril D stagger as a function of the tendon strain ($D_1(\sigma = 0) = D_2(\sigma = 0) \equiv D_0$). For strains larger than 2–3%, the diffraction profile of the stretched tendon can be resolved into two components with different D parameters D_1 (open symbols) and D_2 (closed symbols).

The scanning electron microscope in the normal and quantitative backscattered electron imaging (qBEI) mode was used to view the mineralized microstructure of the tendon in cross sections taken perpendicular to the tendon axis [25]. Samples were embedded in polymethylmethacrylate (PMMA), sectioned with a diamond saw transverse to the fibril direction, polished, and carbon-coated. An overview backscattered electron image of 12 week and 24 week tendons is shown in Fig. 3(a). Lighter regions correspond to a higher degree of mineralization. In both figures an outer envelope of unmineralized tissue (shown by a white line) surrounded the interior but the main difference was the degree of mineralization in the interior region, with the younger tendon having a larger fraction of unmineralized tissue. The interior region of the tendon cross section consisted of highly mineralized and lowly mineralized fiber bundles typically 2–4 μm in

diameter [Fig. 3(b)], as well as the vascular channels and blood vessels which are filled with resin during the embedding process. An empirical cutoff gray level of 26 demarcates resin from tissue (0 ≡ black, 256 ≡ white). The area fraction of unmineralized tissue relative to the total tissue area was 38.5% in the 12 week sample and 5.2% for the 24-week sample [Fig. 3(a)]. We also embedded two tensile-tested samples for each age in PMMA and measured the total unmineralized area fractions. We obtained values of 39.7 ± 0.1 (12 week), 9.8 ± 1.8 (15 week) and 3.5 ± 0.7 (24 week). The mean weight percentage of mineral in the mineralized fiber bundles was about 51.4% (compared to about 55.5% in human trabecular bone [25]).

To interpret our mechanical and structural results, we regard MTLT as a two-fiber composite of brittle mineralized and extensible unmineralized fiber bundles at the microstructural level, in which the mineralized fiber bundles contain mineral particles infiltrated into and onto the surface of the collagen fibrils [13,26]. A fiber composite model for the fracture process in the tissue is shown in Fig. 3(b) [27]. For strains below the low fracture strain of the mineralized fiber bundles (2–3%) the elongation is homogenous across the tendon. For larger strains, the brittle mineralized fibers break and relax back to their unstressed values, and no longer carry tensile load. The load is transferred to the compliant unmineralized fibers, and the elongation occurs faster. The tissue breaks when reaching the fracture strain of the unmineralized fibers. Interestingly, the maximum D period of 70 nm reached in this process is significantly larger than the maximum D period in rat tail tendons [18,19]. In Fig. 3(c), load cycling measurements on MTLT from 15 week old turkeys show a clear transition from bonelike behavior in the initial cycles (when the unmineralized component is still unbroken, and the initial slope is steep and linear) to typical *unmineralized* tendonlike behavior for later cycles (with the S-shaped curve similar to unmineralized collagen [19]), implying that the mineralized component has broken and the unmineralized collagen bears the resulting reduced load.

We plot in Fig. 4 the elastic modulus E (the initial slope) of the stress-strain curve versus the post-yield slope E_{inel}. E_{inel} is observed to be negatively correlated to E, but the data points for the different age categories are not clearly separated. However there exists a trend that tendons from older animals have a higher E but lower E_{inel}. If the fraction of total mineralized tissue ϕ in-

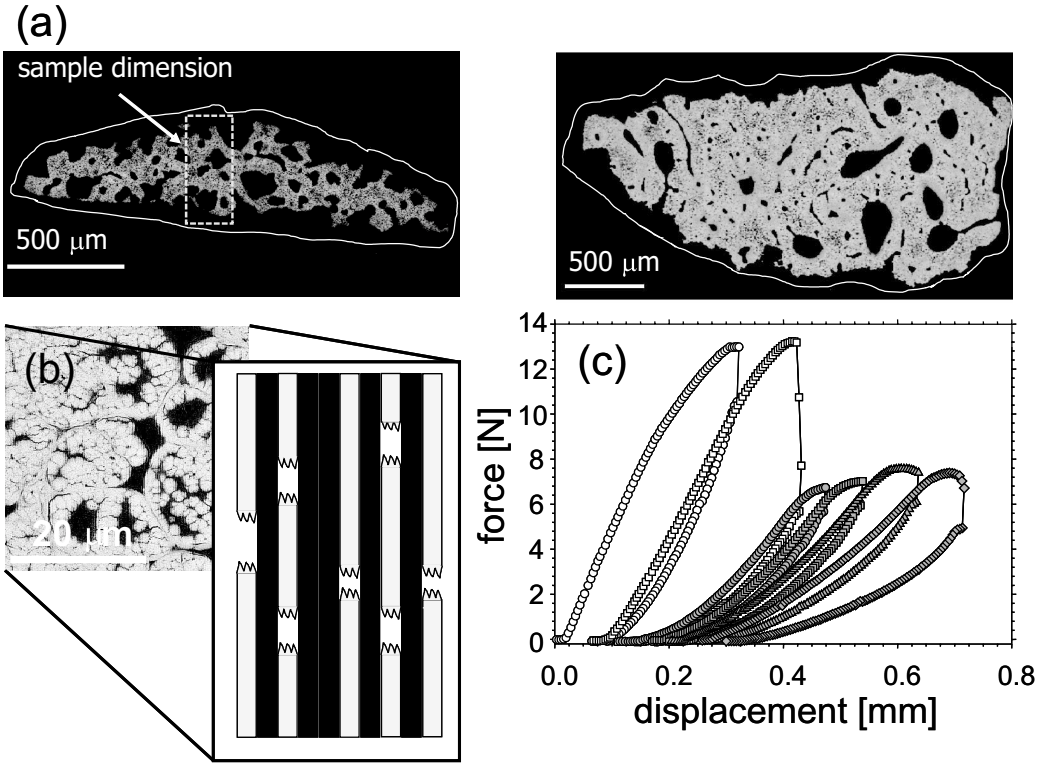

FIG. 3. (a) qBEI images of young (12 week, left) and old (24 week, right) tendons sectioned perpendicular to fiber axis. Lighter regions have higher mineral content. White line demarcates whole tendon; typical sample dimensions shown. (b) High magnification qBEI image of 24 week tendon, and schematic of fracture mechanism. Light-colored mineralized and dark unmineralized fiber bundles are visible in qBEI image. (c) Load cycling measurements on 15 week MTLT: cycles 1, 2: white ○, □ respectively; cycles 3–6: gray ○, □, △, ◇ respectively.

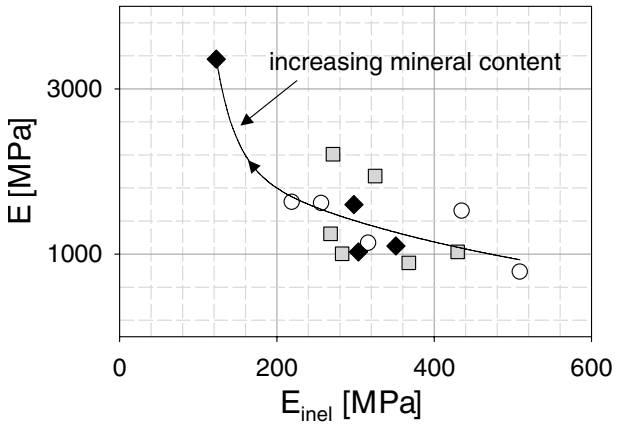

FIG. 4. Plot of the initial slope (elastic modulus E) versus the post-yield slope E_{inel}. White ○ = 12 week, gray □ = 15 week, and filled ◇ = 24 week samples. Arrowed line in the direction of increasing average mineral content.

creases with age, then $\frac{E_{\text{inel}}}{E} = \frac{(1-\phi)(E_c/E_m)}{\phi+(1-\phi)E_c/E_m}$, where ϕ is the volume fraction of mineralized tissue, E_m the modulus of mineralized tissue, and E_c the modulus for unmineralized tissue. The ratio $\frac{E_{\text{inel}}}{E}$ decreases as ϕ increases. The implication of Fig. 4 is that the higher initial stiffness in more mature tendons comes at the expense of increased damage in the post-transition region.

While mineralized turkey tendon is a good model system, structurally and mechanically, for mineralized collagen fibrils, it is not very related to bone, either in terms of the origin of mineralization or the suprafibrillar structures it forms during calcification and vascularization [13]. Both the higher degree of mineralization in bone and its more complex fibril array architecture suggest that mechanisms other than the model proposed here may also play a role in bone. Specifically, mechanisms such as crack bridging [1], microcracking [7], and cement line creep [6] have been observed at higher length scales than the nanometer level considered here [28]. In addition we do not consider here the mechanical influence of changes in the cross-linking of the organic matrix with increasing age, which would be also expected to increase the stiffness and strength [29,30].

To summarize, we carried out a novel direct measurement of the load related structural changes in mineralized collagen at the level of fibrils and fibril arrays, a length scale that has not been investigated in detail so far in the fracture studies of bone and hard tissues. Parallel-fibered mineralized collagen consists of both highly mineralized and weakly mineralized domains. It was shown that this leads to a deformation mechanism where the high initial stiffness is followed by a damage region where we believe the unmineralized component maintains the structural integrity by deforming to a large ultimate fracture strain. The technique provides a way to estimate the actual compliance of mineralized fibrils, in general, for mineralized tissues. The results are of special use in building a comprehensive picture of the failure processes and fracture mechanisms in bone and related mineralized tissues.

We thank H. Amenitsch, T. Schöberl, N. Eidelmann, K. Misof, I. Zizak, G. Dinst, W. Wagermaier, and M. Kerschnitzki for scientific and technical assistance.

[1] R. K. Nalla, J. H. Kinney, and R. O. Ritchie, Nat. Mater. **2**, 164 (2003).
[2] J. B. Thompson *et al.*, Nature (London) **414**, 773 (2001).
[3] S. Weiner and H. D. Wagner, Annu. Rev. Mater. Sci. **28**, 271 (1998).
[4] J.-Y. Rho, L. Kuhn-Spearing, and P. Zioupos, Medical Engineering and Physics **20**, 92 (1998).
[5] R. Lakes, Nature (London) **361**, 511 (1993).
[6] R. Lakes and S. Saha, Science **204**, 501 (1979).
[7] P. Zioupos, Mater. Sci. Eng. **C6**, 33 (1998).
[8] W. E. Caler and D. R. Carter, J. Biomech. **22**, 625 (1989).
[9] M. Fondrk *et al.*, J. Biomech. **21**, 623 (1988).
[10] M. M. Giraud-Guille, Calcif. Tissue Int. **42**, 167 (1988).
[11] S. Weiner, W. Traub, and H. D. Wagner, J. Struct. Biol. **126**, 241 (1999).
[12] W. J. Landis, J. Ultrastruct. Mol. Struct. Res. **94**, 217 (1986).
[13] W. J. Landis *et al.*, Connect. Tissue Res. **43**, 595 (2002).
[14] W. J. Landis *et al.*, J. Bone Miner. Res. **10**, 859 (1995).
[15] T. J. Roberts *et al.*, Science **275**, 1113 (1997).
[16] F. H. Silver *et al.*, Biomacromolecules **2**, 750 (2001).
[17] K. Misof, G. Rapp, and P. Fratzl, Biophys. J. **72**, 1376 (1997).
[18] P. Fratzl *et al.*, J. Struct. Biol. **122**, 119 (1998).
[19] R. Puxkandl *et al.*, Philos. Trans. R. Soc. London B **357**, 191 (2002).
[20] E. Mosler *et al.*, J. Mol. Biol. **182**, 589 (1985).
[21] N. Sasaki and S. Odajima, J. Biomech. **29**, 1131 (1996).
[22] K. S. Borsato and N. Sasaki, J. Biomech. **30**, 955 (1997).
[23] Hodge, in *Aspects of Protein Structure*, edited by G. N. Ramachandran (Academic Press, New York, 1963), p. 289.
[24] S. W. White *et al.*, Nature (London) **266**, 421 (1977).
[25] P. Roschger *et al.*, Bone (N.Y.) **23**, 319 (1998).
[26] W. J. Landis *et al.*, J. Struct. Biol. **117**, 24 (1996).
[27] D. Hull and T. W. Clyne, *An Introduction to Composite Materials* (Cambridge University Press, Cambridge, England, 1996).
[28] J. D. Currey, *Bones: Structure and Mechanics* (Princeton University Press, Princeton, 2002).
[29] M. Yamauchi and E. P. Katz, Connect. Tissue Res. **29**, 81 (1993).
[30] L. Knott, J. F. Tarlton, and A. J. Bailey, Biochem. J. **322**, 535 (1997).